

# Collaborative Deterministic-Diffusion Model for Probabilistic Urban Spatiotemporal Prediction

Zhi Sheng, Yuan Yuan, Yudi Zhang, Depeng Jin, Yong Li

Tsinghua University

y-yuan20@mails.tsinghua.edu.cn, liyong07@tsinghua.edu.cn

## ABSTRACT

Accurate prediction of urban spatiotemporal dynamics is essential for enhancing urban management and decision-making. Existing spatiotemporal prediction models are predominantly deterministic, focusing on primary spatiotemporal patterns. However, those dynamics are highly complex, exhibiting multi-modal distributions that are challenging for deterministic models to capture. In this paper, we highlight the critical role of probabilistic prediction in capturing the uncertainties and complexities inherent in spatiotemporal data. While mainstream probabilistic models can capture uncertainty, they struggle with accurately learning primary patterns and often suffer from computational inefficiency. To address these challenges, we propose CoST, which collaborates deterministic and probabilistic models to improve both predictive accuracy and the ability to handle uncertainty. To achieve this, we design a mean-residual decomposition framework, where the mean value is modeled by a deterministic model, and the residual variations are learned by a probabilistic model, specifically diffusion models. Moreover, we introduce a scale-aware diffusion process, which better accounts for spatially heterogeneous dynamics across different regions. Extensive experiments on eight real-world datasets demonstrate that CoST significantly outperforms existing methods in both deterministic and probabilistic metrics, achieving a 20% improvement with low computational cost. CoST bridges the gap between deterministic precision and probabilistic uncertainty, making a significant advancement in the field of urban spatiotemporal prediction.

## KEYWORDS

Probabilistic prediction, deterministic models, diffusion models

## 1 INTRODUCTION

Accurate prediction of urban spatiotemporal dynamics is crucial for urban management, efficiency optimization, and the development of smart cities [22, 47, 53, 55]. These urban spatiotemporal data encapsulate complex patterns while also exhibiting randomness [4, 11, 26, 42, 55]. Taking traffic flow data as an example, it displays clear temporal and spatial patterns: it peaks during rush hours and is influenced by neighboring regions, while also being prone to random fluctuations caused by events like accidents or extreme weather.

Mainstream urban spatiotemporal prediction methods mainly rely on deterministic models [41, 48, 52, 53, 55]. These models typically use mean absolute error ( $\mathcal{L}_1$ ) or squared error ( $\mathcal{L}_2$ ) between predicted and true values as the loss function. This allows to learn the expected value and capture primary spatiotemporal patterns. However, the data often follow a multi-modal distribution [14, 18], where multiple states can coexist at a given spatiotemporal point.

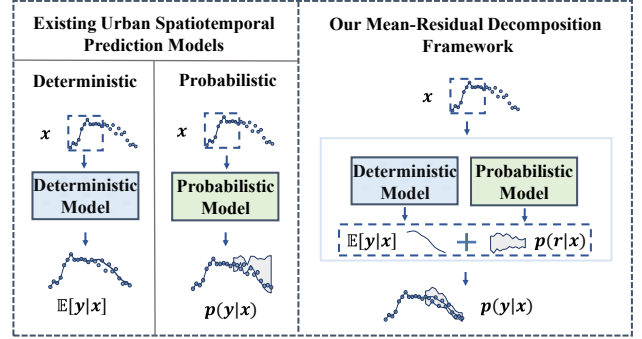


Figure 1: Comparison of existing models with our mean-residual decomposition framework.

For example, in a scenario where a road segment with frequent accidents has an accident rate  $p_1$ , with peak traffic volumes  $y_1$  during normal hours and  $y_2$  during accidents, deterministic models learn a conditional mean:  $\mathbb{E}[y|x] = p_1 \times y_2 + (1 - p_1) \times y_1$ . However, this underestimates the resources needed in congested areas and over-allocates them to free-flowing ones. In contrast, probabilistic methods can address this by modeling multi-modal distributions.

Existing probabilistic models, such as Generative Adversarial Networks (GANs) [13, 17], Variational Autoencoders (VAEs) [25, 27], and Diffusion Models [20, 43], have shown promising performance. These methods aim to learn the full data distribution, capturing both primary patterns (e.g., long-term temporal trends and global spatial patterns) and non-linear variations (e.g., random fluctuations caused by incidental events). However, their focus on modeling uncertainty often limits their ability to accurately capture the primary patterns. Additionally, these models often suffer from inefficiency in real-world deployment. For example, GANs struggle with training challenges and mode collapse [6, 17], while diffusion models require multiple denoising steps for sampling, increasing computational costs [38, 43, 54].

Therefore, we aim to leverage the strengths of both deterministic and probabilistic models to enhance predictive accuracy while effectively capturing uncertainty. However, this is not trivial and faces three challenges: (i) Spatiotemporal data not only exhibits primary spatiotemporal patterns but also involves random fluctuations. (ii) The multi-modal distributions across different spatiotemporal locations are inherently heterogeneous. (iii) Large-scale urban computing and decision-making applications require both computationally efficient and scalable prediction models.

To address the aforementioned challenges, we propose CoST that Collaborates the deterministic model and probabilistic model for urban SpatioTemporal prediction. As illustrated in Figure 1,

we leverage an advanced deterministic spatiotemporal prediction model to capture the primary patterns and predict the conditional mean  $\mathbb{E}(y|x)$ . On this basis, we employ the diffusion model to model the residual distribution  $p(r|x) = p(y - \mathbb{E}(y|x)|x)$ , compensating for the limitations of the mean prediction. Additionally, we propose a scale-aware diffusion process to handle the spatial heterogeneity. To thoroughly evaluate the performance of probabilistic predictions, we conduct experiments on eight real-world datasets, encompassing crowd flows, cellular network traffic, vehicle flow, and traffic speed. We use both deterministic metrics (MAE, RMSE) and probabilistic metrics (CRPS, QICE, IS) for evaluation. Experimental results demonstrate that our model outperforms existing approaches in both predictive performance and computational efficiency. In summary, our main contributions are as follows:

- We propose to collaborate deterministic and probabilistic models for probabilistic urban spatiotemporal prediction, leveraging their strengths in both accuracy and uncertainty handling.
- We propose CoST, a mean-residual decomposition framework where the mean is modeled deterministically and residual variations are learned probabilistically using diffusion models. Additionally, we introduce a scale-aware diffusion process to capture spatial variability in residual distributions.
- We conduct experiments on 8 real-world datasets using comprehensive metrics for evaluation. Results demonstrate that CoST outperforms existing approaches across multiple key metrics, achieving 20% performance improvement with high efficiency.

## 2 RELATED WORK

### 2.1 Urban Spatiotemporal Prediction

Spatiotemporal prediction in urban environments [50, 52, 55] aims to model and forecast the dynamics of urban data, such as traffic flow, cellular network traffic, and energy consumption. Previously, researchers have employed statistical methods (e.g., ARIMA [5]) and traditional machine learning models (e.g., SVM [34], GP [40], and RF [19]) for prediction. Recently, a variety of neural network-based models have been proposed for this task, which can be categorized into deterministic and probabilistic prediction.

### 2.2 Deterministic Prediction

Deterministic prediction of spatiotemporal data is a point estimation approach that assumes a deterministic prediction can be made given the same historical observations. These models are typically trained using loss functions such as MSE or MAE, ensuring that the model learns to predict the conditional mean  $\mathbb{E}[y|x]$  to capture the primary patterns. Existing deep learning-based deterministic forecasting models include MLP-based [36, 41, 57], CNN-based [28, 31, 55], and RNN-based [2, 30, 44, 45] architectures, which are commonly used for their computational efficiency. Additionally, GNN-based models [1, 1, 3, 15, 22] have been developed to capture spatial dependencies in graph-structured data, while Transformer-based models [8, 10, 21, 51] excel at capturing complex dynamic patterns.

### 2.3 Probabilistic Prediction

The core of probabilistic prediction lies in constructing a conditional probability distribution  $p(y|x)$ , which quantifies the uncertainty of the prediction rather than merely providing a single deterministic value [43, 49]. Unlike deterministic prediction models, these models assess the reliability of the predictions through probabilistic representations like quantiles or confidence intervals. Early applications typically employ Bayesian networks. In recent years, with the development of generative models, approaches based on GAN [23, 39, 56], VAE [9, 12, 58], and diffusion models [7, 29, 43] have made significant advancements, owing to their powerful data distribution modeling capabilities. However, deterministic models still dominate in related research, and probabilistic prediction models remain relatively underexplored. This study aims to leverage the strengths of both deterministic and probabilistic models to achieve efficient probabilistic predictions.

## 3 PRELIMINARY

### 3.1 Problem Formulation

Urban spatiotemporal prediction aims to predict future variations based on historical observations. The urban spatiotemporal data is typically represented as a multi-dimensional tensor  $\mathbf{x} \in \mathbb{R}^{T \times K \times C}$ , where  $T$  denotes the temporal dimension,  $K$  represents the spatial dimension, and  $C$  is the feature dimension. The format typically includes two types: grid-based data and graph-based data.

For grid-based data, the spatial dimension  $K$  can be expressed in a two-dimensional form as  $H \times W$ , where  $H$  and  $W$  denote the height and width, respectively.

For graph-based data,  $K$  represents the number of nodes in the graph structure. These nodes are located within a spatial topological structure denoted as  $\mathcal{G} = (\mathcal{V}, \mathcal{E}, \mathcal{A})$ . Here,  $\mathcal{V}$  is the set of all nodes,  $\mathcal{E}$  is the set of edges connecting the nodes. In addition,  $\mathcal{A}$  is the adjacency matrix of graph  $\mathcal{G}$ . Its elements  $a_{ij}$  show if there's an edge between node  $i$  and  $j$  in  $\mathcal{V}$ ,  $a_{ij} = 1$  when there's an edge and  $a_{ij} = 0$  otherwise.

### 3.2 Diffusion-based Probabilistic Prediction

The diffusion-based urban spatiotemporal model is a conditional probabilistic model, consisting of a forward process and a reverse process. In the forward process, noise is added incrementally to target data  $\mathbf{x}_0^{ta}$  according to a predefined noise schedule  $\{\beta_n\}_{n=1}^N$ , gradually transforming the data distribution into a standard Gaussian distribution  $\mathcal{N}(\mathbf{0}, \mathbf{I})$ . At any diffusion step, the corrupted target data can be computed using the one-step forward equation:

$$\mathbf{x}_n^{ta} = \sqrt{\bar{\alpha}_n} \mathbf{x}_0^{ta} + \sqrt{1 - \bar{\alpha}_n} \epsilon, \quad \epsilon \sim \mathcal{N}(\mathbf{0}, \mathbf{I}), \quad (1)$$

where  $\bar{\alpha}_n = \prod_{i=1}^n \alpha_i$  and  $\alpha_n = 1 - \beta_n$ . In the reverse process, we first sample  $\mathbf{x}_N^{ta}$  from the standard Gaussian distribution  $\mathcal{N}(\mathbf{0}, \mathbf{I})$  and denoise it through the following Markov process:

$$\begin{aligned} p_\theta(\mathbf{x}_{0:N}^{ta}) &:= p(\mathbf{x}_N^{ta}) \prod_{n=1}^N p_\theta(\mathbf{x}_{n-1}^{ta} | \mathbf{x}_n^{ta}, \mathbf{x}_0^{co}), \\ p_\theta(\mathbf{x}_{n-1}^{ta} | \mathbf{x}_n^{ta}) &:= \mathcal{N}(\mathbf{x}_{n-1}^{ta}; \mu_\theta(\mathbf{x}_n^{ta}, n | \mathbf{x}_0^{co}), \Sigma_\theta(\mathbf{x}_n^{ta}, n)), \\ \mu_\theta(\mathbf{x}_n^{ta}, n | \mathbf{x}_0^{co}) &= \frac{1}{\sqrt{\bar{\alpha}_n}} \left( \mathbf{x}_n^{ta} - \frac{\beta_n}{\sqrt{1 - \bar{\alpha}_n}} \epsilon_\theta(\mathbf{x}_n^{ta}, n | \mathbf{x}_0^{co}) \right) \end{aligned} \quad (2)$$

where the variance  $\Sigma_\theta(\mathbf{x}_n^{ta}, n) = \frac{1-\bar{\alpha}_{n-1}}{1-\bar{\alpha}_n}\beta_n$ , and  $\epsilon_\theta(\mathbf{x}_n^{ta}, n|\mathbf{x}_0^{co})$  is predicted by the denoising network which is trained by the loss function below:

$$\mathcal{L}(\theta) = \mathbb{E}_{n, \mathbf{x}_0, \epsilon} \left[ \left\| \epsilon - \epsilon_\theta(\mathbf{x}_n^{ta}, n|\mathbf{x}_0^{co}) \right\|_2^2 \right]. \quad (3)$$

### 3.3 Evaluation of Probabilistic Prediction

To comprehensively evaluate probabilistic prediction, it is essential to consider two key dimensions:

- **Data Distribution**—the predicted distribution should align with the empirical data distribution.
- **Prediction Usability**—A reliable prediction interval has a high probability of containing the true future values, while a sharp interval provides a more precise estimate.

Existing studies predominantly rely on Continuous Ranked Probability Score (CRPS) to provide a measure of the distribution discrepancy, while deterministic metrics such as MAE and RMSE to capture point estimation errors. However, these metrics fail to systematically evaluate: (i) Whether the learned distribution accurately covers the data across different quantile intervals, particularly when dealing with multi-modal distributions; (ii) Whether the interval width appropriately reflects real uncertainty. To address these challenges, we introduce two more evaluation metrics, Quantile Interval Coverage Error (QICE) and Interval Score (IS).

**QICE.** QICE is first proposed in [18] for regression tasks. This metric is intended to assess the mean absolute deviation between the proportion of true data points within each quantile interval (QI) and the ideal proportion. Specially, for each sample point  $y$ , after obtaining a sufficient number of predicted values  $\hat{y}$ , these predictions are divided into  $M_{QIs}$  equally-sized QIs. Then the QICE is computed according to the following formula:

$$\begin{aligned} \text{QICE} &:= \frac{1}{M_{QIs}} \sum_{m=1}^{M_{QIs}} \left| r_m - \frac{1}{M_{QIs}} \right|, \\ r_m &= \frac{1}{N} \sum_{n=1}^N \mathbb{1}_{y_n \geq \hat{y}_n^{\text{low}_m}} \cdot \mathbb{1}_{y_n \leq \hat{y}_n^{\text{high}_m}}, \end{aligned} \quad (4)$$

where  $\hat{y}_n^{\text{low}_m}$  and  $\hat{y}_n^{\text{high}_m}$  represents the lower and upper bound of the  $m$ -th quantile interval for  $y_n$ . When the true distribution aligns with the predicted distribution,  $\frac{1}{M_{QIs}}$  of the observation data will fall into each QI, achieving an optimal QICE value of 0. Smaller values of QICE indicate a closer match between the learned distribution and the true distribution.

**IS.** The IS is a scoring metric designed to evaluate the quality of probabilistic prediction intervals (PIs). It is defined and systematically studied in [16]. This metric jointly considers two critical aspects: the sharpness and coverage ability of the prediction interval. The computation of IS can be formulated as follows:

$$\text{IS} := \frac{1}{N} \sum_{n=1}^N \left[ (u_n^\alpha - l_n^\alpha) + \frac{2}{\alpha} (l_n^\alpha - y_n) \mathbb{1}_{y_n < l_n^\alpha} + \frac{2}{\alpha} (y_n - u_n^\alpha) \mathbb{1}_{y_n > u_n^\alpha} \right], \quad (5)$$

where  $u_n^\alpha$  and  $l_n^\alpha$  are the upper and lower endpoints of the central  $(1 - \alpha) \times 100\%$  prediction interval for the  $n$ -th data point, which

are the predictive quantiles at levels  $1 - \frac{\alpha}{2}$  and  $\frac{\alpha}{2}$  respectively;  $y_n$  is the actual value corresponding to the  $n$ -th data point. The final prediction results are rewarded for having a narrower prediction interval. If the observed value falls outside the prediction interval, a penalty is incurred, and the severity of the penalty is determined by the parameter  $\alpha$ . Thus, a lower IS indicates better performance.

## 4 METHODOLOGY

To achieve effective probabilistic predictions, we propose CoST that simultaneously leverages the advantages of both deterministic and probabilistic models. Our approach involves two stages. In the first stage, the deterministic model is pretrained to predict the conditional mean that captures the primary patterns. In the second stage, the parameters of the deterministic model are frozen, and the scale-aware diffusion model, constrained by a customized fluctuation scale, is jointly trained to model residual distributions that reflect random fluctuations. Figure 2 illustrates an overview of our model.

### 4.1 Mean-Residual Decomposition

For urban spatiotemporal probabilistic prediction, current approaches typically employ a single probabilistic model to capture the full distribution of data, incorporating both the primary spatiotemporal patterns and the random fluctuations. However, it is challenging to model both of these distributions. Inspired by [32] and the Reynolds decomposition in fluid dynamics [35], we propose to decompose the target data  $\mathbf{x}^{ta}$  as follows:

$$\mathbf{x}^{ta} = \underbrace{\mathbb{E}[\mathbf{x}^{ta}|\mathbf{x}^{co}]}_{:=\boldsymbol{\mu}(\text{Deterministic})} + \underbrace{(\mathbf{x}^{ta} - \mathbb{E}[\mathbf{x}^{ta}|\mathbf{x}^{co}])}_{:=\mathbf{r}(\text{Probabilistic})}, \quad (6)$$

where  $\boldsymbol{\mu}$  is the conditional mean representing the primary patterns, and  $\mathbf{r}$  is the residual representing the random variations. Our core idea is that if a deterministic model can accurately predict the conditional mean, that is,  $\boldsymbol{\mu} \approx \mathbb{E}_\theta[\mathbf{x}^{ta}|\mathbf{x}]$ , then the probabilistic model only needs to focus on learning the simpler residual distribution, thus combining the strengths of both models to enhance the probabilistic prediction capability.

### 4.2 Mean Prediction via Deterministic Model

We require a deterministic model that can accurately predict the conditional mean to align with our research hypothesis, and also maintain high predictive efficiency to avoid additional increases in training and inference time. Therefore, we select the MLP-based STID model as our mean prediction module. In the first stage of training, we pretrain the model for 50 epochs to effectively capture the primary spatiotemporal patterns. Specifically, we input historical conditional data  $\mathbf{x}^{co}$  into the STID model to obtain the conditional mean output  $\mathbb{E}_\theta[\mathbf{x}^{ta}|\mathbf{x}^{co}]$ .

The STID model is pretrained by optimizing the following loss function:

$$\mathcal{L}_2 = \left\| \mathbb{E}_\theta[\mathbf{x}^{ta}|\mathbf{x}^{co}] - \mathbf{x}^{ta} \right\|_2^2. \quad (7)$$

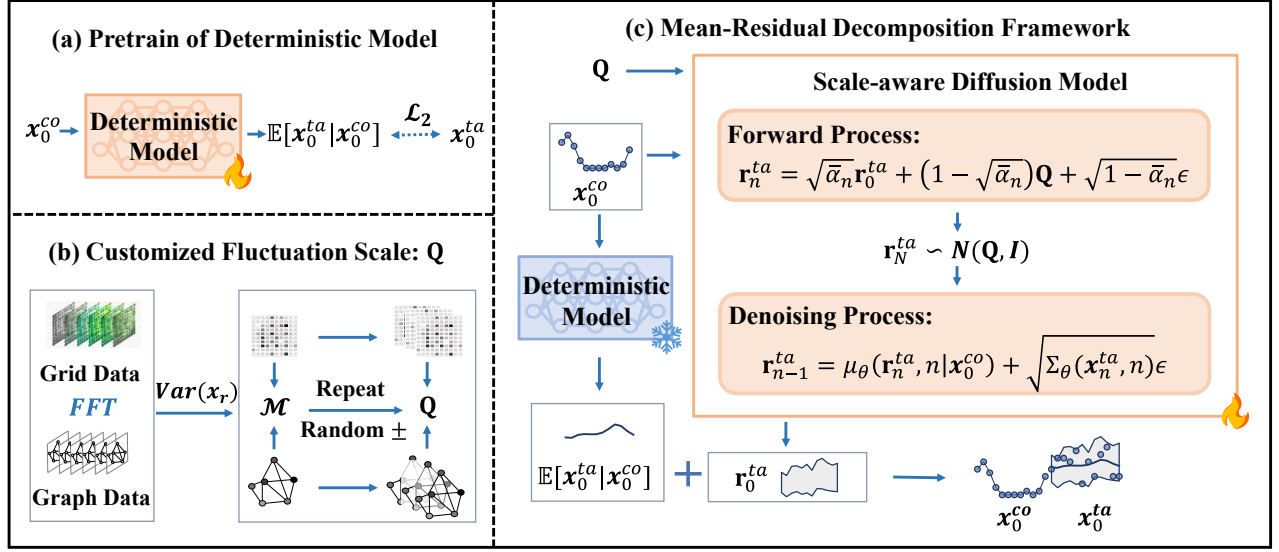


Figure 2: The overview of CoST. (a) illustrates the pretraining process of the deterministic prediction model. (b) demonstrates the computation of the Customized Fluctuation Scale. (c) presents the overall framework of the mean-residual decomposition.

### 4.3 Residual Learning via Diffusion Model

Diffusion models have achieved significant success in probabilistic modeling. In this work, we employ a diffusion model for probabilistic prediction, training it to learn the residual distribution:

$$\mathbf{r}_{ta} = \mathbf{x}^{ta} - \mathbb{E}[\mathbf{x}^{ta} | \mathbf{x}^{co}]. \quad (8)$$

Consequently, the target data  $\mathbf{x}^{ta}$  for diffusion models in Eqs. (8), (2), and (3) is replaced by  $\mathbf{r}_{ta}$ . The residual distribution of urban spatiotemporal data is not independently and identically distributed (i.i.d.) nor does it follow a fixed distribution, such as  $\mathcal{N}(0, \sigma)$ . Instead, it often exhibits complex spatiotemporal dependence and heterogeneity. So we consider both temporal residual learning and spatial residual learning.

**Temporal Residual Learning.** For urban spatiotemporal data, the residual distribution varies at different time points. For example, fluctuations are lower at night and higher during the day, with uncertainty varying between weekends and weekdays. To model this, we incorporate the timestamp information as the condition for the denoising process. Meanwhile, the residual distribution can also be affected by sudden weather changes or public events. To capture these real-time changes, we concatenate the context data  $\mathbf{x}_0^{co}$  with noised target residual  $\mathbf{r}_n^{ta}$  as the input. The noise is not added to  $\mathbf{x}_0^{co}$  and  $\mathbf{r}_n^{ta}$  during the diffusion training and inference.

**Spatial Residual Learning.** In areas with frequent traffic accidents, fluctuations tend to be more pronounced and may induce anomalous variations in adjacent regions, thus affecting their distributions. For spatial dependence modeling, the model learns a spatial embedding for each location, following the STID approach. Additionally, we propose a scale-aware diffusion process to further distinguish the heterogeneity for different regions. In this section, we detail the calculation of  $\mathbf{Q}$  and how it is integrated into the scale-aware diffusion process.

(i) **Customized Fluctuation Scale.** Specifically, we apply the Fast Fourier Transform (FFT) to spatiotemporal sequences in the training set to quantify fluctuation levels in different regions and use the custom scale  $\mathbf{Q}$  as input to account for spatial differences in residual. Specifically, we first employ FFT to extract the fluctuation components for each region within the training set. The detailed steps are as follows:

$$\begin{aligned} A_k &= |\text{FFT}(\mathbf{x})_k|, & \phi_k &= \phi(\text{FFT}(\mathbf{x})_k), \\ A_{\max} &= \max_{k \in \{1, \dots, \lfloor \frac{L}{2} \rfloor + 1\}} A_k, \\ \mathcal{K} &= \left\{ k \in \left\{ 1, \dots, \left\lfloor \frac{L}{2} \right\rfloor + 1 \right\} : A_k < 0.1 \times A_{\max} \right\}, \\ \mathbf{x}_r[i] &= \sum_{k \in \mathcal{K}} A_k \left[ \cos(2\pi \mathbf{f}_k i + \phi_k) \right. \\ &\quad \left. + \cos(2\pi \bar{\mathbf{f}}_k i + \bar{\phi}_k) \right], \end{aligned} \quad (9)$$

where  $A_k, \phi_k$  represent the amplitude and phase of the  $k$ -th frequency component.  $L$  is the temporal length of the training set.  $A_{\max}$  is the maximum amplitude among the components, obtained using the max operator.  $\mathcal{K}$  represents the set of indices for the selected residual components.  $\mathbf{f}_k$  is the frequency of the  $k$ -th component.  $\bar{\mathbf{f}}_k, \bar{\phi}_k$  represent the conjugate components.  $\mathbf{x}_r$  ref to the extracted residual component of the training set. We then compute the variance  $\sigma_k^2$  of the residual sequence for each location  $k$  and expand it to match the shape as  $\mathbf{r}_0^{ta} \in \mathbb{R}^{B \times K \times P}$ , where  $B$  represents the batch size. And we can get the variance tensor  $\mathcal{M}$ :

$$\begin{aligned} \mathcal{M}_{b,k,p} &= \sigma_k^2, \\ \forall b \in \{1, \dots, B\}, \forall k \in \{1, \dots, K\}, \forall p \in \{1, \dots, P\}. \end{aligned} \quad (10)$$

The residual fluctuations are bidirectional, encompassing both positive and negative variations, so we generate a random sign tensor

**Algorithm 1** Training

- 
- 1: **Stage 1: Pretraining of Deterministic Model**  $\mathbb{E}_\theta$
  - 2: **repeat**
  - 3:   Estimate the conditional mean  $\mathbb{E}_\theta[\mathbf{x}_0^{ta}|\mathbf{x}_0^{co}]$ .
  - 4:   Update  $\mathbb{E}_\theta$  using the following loss function:
 
$$\mathcal{L}_2 = \|\mathbb{E}_\theta[\mathbf{x}_0^{ta}|\mathbf{x}_0^{co}] - \mathbf{x}_0^{ta}\|_2^2$$
  - 5: **until** The model has converged.
  - 6: **Stage 2: Training of Diffusion Model**  $\epsilon_\theta$
  - 7: **repeat**
  - 8:   Initialize  $n \sim \text{Uniform}(1, \dots, N)$  and  $\epsilon \sim \mathcal{N}(0, I)$ .
  - 9:   Calculate the target  $\mathbf{r}_0^{ta} = \mathbf{x}_0^{ta} - \mathbb{E}_\theta[\mathbf{x}_0^{ta}|\mathbf{x}_0^{co}]$ .
  - 10:   Calculate noisy targets  $\mathbf{r}_n^{ta}$  using Eq. (13).
  - 11:   Update  $\epsilon_\theta$  using the following loss function:
 
$$\mathcal{L}(\theta) = \|\epsilon - \epsilon_\theta(\mathbf{r}_n^{ta}, n|\mathbf{x}_0^{co})\|_2^2$$
  - 12: **until** The model has converged.
- 

$\mathbf{S} \in \mathbb{R}^{B \times K \times P}$  for  $\mathcal{M}$ , where each element  $S_{b,k,p}$  of  $\mathbf{S}$  is sampled from a Bernoulli distribution with  $p = 0.5$ . The customized fluctuation scale  $\mathbf{Q}$  is then defined as:

$$\begin{aligned} \mathbf{Q}_{b,k,p} &= S_{b,k,p} \times \mathcal{M}_{b,k,p}, \\ \forall b \in \{1, \dots, B\}, \forall k \in \{1, \dots, K\}, \forall p \in \{1, \dots, P\}. \end{aligned} \quad (11)$$

Then  $\mathbf{Q}$  is used as the input of the denoising network.

**(ii) Scale-aware Diffusion Process.**

The vanilla diffusion models typically model all regions as the same  $\mathcal{N}(0, I)$  distribution at the end of the diffusion process, failing to distinguish the differences among regions. To further model the differences of residual distribution across various regions, we adopt the technique proposed by [18] to make the residual learning region-specific conditioned on  $\mathbf{Q}$ . Specially, we have calculated the customized fluctuation scale  $\mathbf{Q}$ , and We redefined the noise distribution at the endpoint of the diffusion process as follows:

$$p(\mathbf{r}_N^{ta}) = \mathcal{N}(\mathbf{Q}, I), \quad (12)$$

Accordingly, the Eq 13 in the forward process is rewritten as:

$$\mathbf{r}_n^{ta} = \sqrt{\bar{\alpha}_n} \mathbf{r}_0^{ta} + (1 - \sqrt{\bar{\alpha}_n}) \mathbf{Q} + \sqrt{1 - \bar{\alpha}_n} \epsilon, \quad \epsilon \sim \mathcal{N}(0, I). \quad (13)$$

And in the denoising process, we sample  $\mathbf{r}_N^{ta}$  from  $\mathcal{N}(\mathbf{Q}, I)$ , and denoise it use Eq (2), the computation of  $\mu_\theta(\mathbf{r}_n^{ta}, n|\mathbf{x}_0^{co})$  in Eq 2 is modified as:

$$\mu_\theta(\mathbf{r}_n^{ta}, n|\mathbf{x}_0^{co}) = \frac{1}{\sqrt{\bar{\alpha}_n}} \left( \mathbf{r}_n^{ta} - \frac{\beta_n}{\sqrt{1 - \bar{\alpha}_n}} \epsilon_\theta(\mathbf{r}_n^{ta}, n|\mathbf{x}_0^{co}) \right) + \left( 1 - \frac{1}{\sqrt{\bar{\alpha}_n}} \right) \mathbf{Q}. \quad (14)$$

This approach enables the diffusion process to be governed by the  $\mathbf{Q}$  values at each region, leading to more effective utilization of the customized scale conditions.

**4.4 Training and Inference**

**Training.** Our training process is a two-stage procedure. We first pretrain the deterministic model STID to enable it to predict the conditional mean. Subsequently, we train the diffusion mode to learn the distribution of residuals, where the residuals are calculated as the difference between the true values and the conditional mean

**Algorithm 2** Inference

- 
- 1: **Input:** Context data  $\mathbf{x}_0^{co}$ , customized fluctuation scale  $\mathbf{Q}$ , trained diffusion model  $\epsilon_\theta$ , trained deterministic model  $\mathbb{E}_\theta$
  - 2: **Output:** Target data  $\mathbf{x}_0^{ta}$
  - 3: Estimate the conditional mean  $\mathbb{E}_\theta[\mathbf{x}_0^{ta}|\mathbf{x}_0^{co}]$
  - 4: Sample  $\mathbf{r}_N^{ta}$  from  $\epsilon \sim \mathcal{N}(\mathbf{S}, I)$
  - 5: **for**  $n = N$  to 1 **do**
  - 6:   Estimate the noise  $\epsilon_\theta(\mathbf{r}_n^{ta}, n|\mathbf{x}_0^{co})$
  - 7:   Calculate the  $\mu_\theta(\mathbf{r}_n^{ta}, n|\mathbf{x}_0^{co})$  using Eq. (14)
  - 8:   Sample  $\mathbf{r}_{n-1}^{ta}$  using Eq. (2)
  - 9: **end for**
  - 10: **Return:**  $\mathbf{x}_0^{ta} = \mathbb{E}_\theta[\mathbf{x}_0^{ta}|\mathbf{x}_0^{co}] + \mathbf{r}_0^{ta}$
- 

predicted by the pretrained STID model with frozen parameters. The detailed training procedure is presented in Algorithm 1.

**Inference.** The inference process of the model consists of two paths: one utilizes the pretrained STID model to predict the conditional mean, while the other uses the diffusion model to predict the residuals. The final sample is obtained by summing the results of both paths. This process is detailed in Algorithm 2.

**5 PERFORMANCE EVALUATIONS****5.1 Experimental Settings**

**Datasets.** To validate the effectiveness and generalizability of our method, we use seven real-world datasets across four categories, each with different spatiotemporal granularities, covering information on crowd flow (CrowdBJ and CrowdBM), cellular network traffic (CellularNJ and CellularSH), vehicle flow (TaxiBJ and BikeDC), and traffic speed (Los-Speed). All datasets are split into training, validation, and test sets in a 6:2:2 ratio, and all datasets are standardized during training. Detailed information on the datasets can be found in Table 6.

**Baselines.** we select six of the most widely recognized and state-of-the-art models in the spatiotemporal domain as our baselines, including:

- **D3VAE [27]:** Aims at short-period and noisy time series forecasting. It combines generative modeling with a bidirectional variational auto-encoder, integrating diffusion, denoising, and disentanglement.
- **DiffSTG [46]:** First applies diffusion models to spatiotemporal graph forecasting. By combining STGNNs and diffusion models, it reduces prediction errors and improves uncertainty modeling.
- **TimeGrad [37]:** An autoregressive model based on diffusion models. It conducts probabilistic forecasting for multivariate time series and performs well on real-world datasets.
- **CSDI [43]:** Utilizes score-based diffusion models for time series imputation. It can leverage the correlations of observed values and also shows remarkable results on prediction tasks.
- **Dyffusion [38]:** A training method for diffusion models in probabilistic spatiotemporal forecasting. It combines data temporal dynamics with diffusion steps and performs well in complex dynamics forecasting.

**Table 1: Short-term prediction results on five datasets in terms of CRPS, QICE, and IS. Bold indicates the best performance, while underlining denotes the second-best.**

Model	CellularSH			BikeDC			TaxiBJ			CrowdBJ			Los-Speed		
	CRPS	QICE	IS	CRPS	QICE	IS	CRPS	QICE	IS	CRPS	QICE	IS	CRPS	QICE	IS
D3VAE	0.856	0.105	1.73	0.785	0.157	8.77	0.433	0.160	985.7	0.668	0.099	53.6	0.119	0.089	90.5
DiffSTG	0.303	0.078	0.526	0.692	0.157	8.08	0.299	0.074	416.5	0.436	0.089	32.1	0.078	0.045	50.9
TimeGrad	0.489	0.143	0.759	<u>0.469</u>	0.130	5.65	0.170	0.102	213.2	0.385	0.113	48.6	<b>0.031</b>	0.098	<b>20.8</b>
CSDI	<u>0.200</u>	<u>0.052</u>	<u>0.295</u>	0.529	<u>0.057</u>	<u>4.79</u>	0.122	<u>0.048</u>	121.8	0.306	<u>0.028</u>	<u>16.4</u>	0.059	0.026	30.8
NPDiff	0.201	0.106	0.627	<b>0.442</b>	0.066	7.11	0.222	0.112	474.1	<u>0.287</u>	0.120	34.5	0.057	0.023	<u>30.5</u>
DyDiffusion <sup>1</sup>	0.230	0.096	0.573	0.573	0.079	6.46	<b>0.084</b>	0.054	<u>99.5</u>	-	-	-	-	-	-
<b>CoST</b>	<b>0.149</b>	<b>0.014</b>	<b>0.216</b>	0.534	<b>0.042</b>	<b>4.474</b>	<u>0.100</u>	<b>0.023</b>	<b>95.3</b>	<b>0.215</b>	<b>0.014</b>	<b>11.5</b>	<u>0.056</u>	<b>0.023</b>	32.0

<sup>1</sup> DyDiffusion can only be applied to grid-format data.

**Table 2: Short-term prediction results on four datasets in terms of MAE and RMSE. Bold indicates the best performance, while underlining denotes the second-best.**

Model	CellularSH		BikeDC		TaxiBJ		CrowdBJ	
	MAE	RMSE	MAE	RMSE	MAE	RMSE	MAE	RMSE
D3VAE	0.186	0.373	0.871	3.59	49.3	84.8	5.16	10.1
DiffSTG	0.066	0.103	0.770	4.02	41.8	69.4	3.68	6.63
TimeGrad	0.047	<u>0.053</u>	0.843	<b>1.07</b>	29.1	34.1	4.37	5.43
CSDI	0.044	0.075	0.592	3.10	18.2	31.6	2.71	5.51
NPDiff	<u>0.037</u>	0.057	<b>0.435</b>	1.90	26.7	52.2	<u>2.05</u>	<u>3.27</u>
DyDiffusion	0.050	0.072	<u>0.480</u>	<u>1.37</u>	<b>12.3</b>	<b>18.0</b>	-	-
<b>CoST</b>	<b>0.034</b>	<b>0.052</b>	0.492	1.76	<u>15.1</u>	<u>25.6</u>	<b>1.92</b>	<b>3.04</b>

- **NPDiff** [42]: A general noise prior framework for cellular traffic prediction. It uses the data dynamics to calculate noise prior for the denoising process and achieve effective performance.

Since the dataset contains some data with a grid structure, we construct adjacency matrixes based on the adjacency relationships to support baseline models that rely on graph structures.

**Metrics.** To evaluate the performance, we employed two deterministic metrics, MAE and RMSE, along with three probabilistic metrics: CRPS, QICE, IS. For QICE, we set the number of QIs, denoted as  $M_{QIs}$ , to 10. For IS, we choose a confidence level of 90%, that is,  $\alpha = 0.1$ .

**Experimental Configuration.** In our experiment, for our model, we set the training maximum epoch for both the STID deterministic model and the diffusion model to 50, with early stopping based on patience of 5 for both models. During training, we set the initial learning rate to 0.001, and after 20 epochs, we adjust it to  $4e-4$ . We use the Adam optimizer with a weight decay of  $1e-6$ . For the diffusion model, we set the validation set sampling number to 3, and the average metric computed over these samples is used as the criterion for early stopping. For the baseline models, we set the maximum training epoch to 100 and the early stopping patience also to 5. We set the number of samples to 50 for computing the experimental results presented in the paper. In terms of model architecture, we set the encoder layer number for the STID deterministic model to 4, with an embedding dimension of 32. In the denoising network of

**Table 3: Long-term prediction results on four datasets in terms of CRPS, QICE, and IS. Bold indicates the best performance, while underlining denotes the second-best.**

Model	CellularNJ			CrowdBJ			CrowdBM			Los-Speed		
	CRPS	QICE	IS	CRPS	QICE	IS	CRPS	QICE	IS	CRPS	QICE	IS
D3VAE	0.856	0.105	1.729	0.710	0.109	63.9	0.674	0.108	152.3	0.138	0.101	113.2
DiffSTG	0.374	0.107	0.923	0.370	0.094	31.3	0.400	0.073	67.1	<u>0.124</u>	<u>0.080</u>	104.6
TimeGrad	0.245	0.075	0.408	0.371	0.073	32.4	0.237	<u>0.049</u>	33.9	0.192	0.081	98.8
CSDI	<u>0.158</u>	<u>0.045</u>	<b>0.216</b>	<u>0.229</u>	<u>0.038</u>	<u>12.0</u>	<u>0.235</u>	<u>0.052</u>	<u>33.7</u>	0.134	0.090	59.2
NPDiff	0.204	0.102	0.611	0.288	0.114	33.6	0.331	0.111	90.8	1.366	0.126	950.4
DyDiffusion	0.308	0.086	0.550	-	-	-	-	-	-	-	-	-
<b>CoST</b>	<b>0.158</b>	<b>0.016</b>	<u>0.218</u>	<b>0.217</b>	<b>0.011</b>	<b>11.5</b>	<u>0.235</u>	<b>0.009</b>	<b>31.2</b>	<b>0.090</b>	<b>0.038</b>	<u>65.3</u>

the diffusion model, we set the encoder layer number to 8, and the embedding dimension is 128. We set the maximum diffusion steps  $N$  for the diffusion model to 50, with a linear noise schedule from  $\beta_1 = 0.0001$  to the maximum  $\beta_N = 0.5$ .

## 5.2 Short-Term Prediction

**Setups.** We define the short-term prediction task as a 12-step ahead prediction based on the previous 12 steps, following [42, 46]. Since the temporal granularity varies across datasets, the actual time duration corresponding to these 12 steps differs accordingly.

**Results of Probabilistic Metrics.** Table 1 presents the results of probabilistic metrics for selected datasets. Due to space constraints, the remaining results can be found in the Appendix Table 7. As shown in Table 1, our model achieves the best performance across various types of datasets, including crowd flow, cellular network traffic, bike flow, taxi flow, and traffic speed. Compared to the best-performing baseline methods on each dataset, our model demonstrates an average improvement of 38% in CRPS and QICE metrics, indicating its superior ability to accurately capture the true distribution characteristics. Moreover, our model achieves a 11% improvement in the IS metric, suggesting that its prediction intervals not only maintain compactness but also exhibit higher coverage, thereby better reflecting the uncertainty of data. Although certain individual metrics may not reach the optimal level on specific datasets, our model consistently maintains performance comparable to the best methods. TimeGrad performs better on the Los-Speed dataset, likely due to its lower dynamic nature and smaller fluctuations, which suits autoregressive models better.

**Table 4: Long-term prediction results on four datasets in terms of MAE and RMSE. Bold indicates the best performance, while underlining denotes the second-best.**

Model	CellularNJ		CrowdBJ		CrowdBM		Los-Speed	
	MAE	RMSE	MAE	RMSE	MAE	RMSE	MAE	RMSE
D3VAE	0.186	0.373	5.63	11.4	12.4	28.2	9.43	<u>13.3</u>
DiffSTG	0.078	0.125	3.04	6.37	7.59	18.8	<u>7.77</u>	14.2
TimeGrad	0.058	0.072	3.48	4.83	5.25	<b>7.40</b>	18.2	22.3
CSDI	<b>0.035</b>	0.057	<u>1.99</u>	3.64	<b>4.64</b>	12.4	11.3	15.0
NPDiff	0.037	<u>0.057</u>	2.06	<u>3.28</u>	5.44	13.8	46.0	58.3
DyDiffusion	0.047	0.066	-	-	-	-	-	-
<b>CoST</b>	<u>0.035</u>	<b>0.053</b>	<b>1.92</b>	<b>3.05</b>	<u>4.74</u>	<u>11.2</u>	<b>5.98</b>	<b>10.8</b>

**Results of Deterministic Metrics.** We also conduct a comparative analysis of the deterministic error between the predicted sample mean and the observation values to assess the offset between the predicted center and the ground truth. Table 2 presents a subset of the results, with more detailed information available in Appendix Table 7. The experimental results demonstrate that our method consistently outperforms others across most datasets, achieving an average reduction of 7% in MAE and 4.5% in RMSE. This indicates that, with the support of the current advanced conditional mean prediction model, our approach can effectively capture the primary patterns compared to other probabilistic baseline models.

### 5.3 Long-Term Prediction

**Setups.** In addition to the 12-step prediction task which is the most typical setup for urban spatiotemporal prediction, we also conduct long-term prediction experiments on four. We define the long-term prediction task as a 64-step ahead prediction based on the previous 64 steps, following [24, 33, 52].

**Results of Probabilistic Metrics.** As shown in Table 3, our model demonstrates exceptional long-term prediction capability. It is worth noting that our model is based on an MLP architecture. Although some individual metrics are slightly inferior to CSDI based on Transformer, which excels at modeling long-term dependencies, our model outperforms them overall. Furthermore, in terms of training efficiency and inference speed, it significantly outperforms it, as detailed in Section 5.5.

**Results of Deterministic Error Metrics.** As shown in Table 4, our model also significantly outperforms other models on deterministic metrics. Compared to the best baseline, our approach achieves an average reduction of 6.5% in MAE and 3.45% in RMSE.

### 5.4 Ablation Study

we conduct an ablation on each proposed module in our model to further evaluate the influence. Specifically, we constructed three variant models by progressively removing key components from the original architecture: **(w/o c)**: The scale-aware diffusion process module is removed; **(w/o q)**: The customized fluctuation scale is excluded as a prior condition; **(w/o m)**: The conditional mean prediction module is eliminated, allowing the model to rely solely on the diffusion model for training. We conducted experiments on two datasets and visualize the results in terms of CRPS and IS metrics, as illustrated in Figure 3. The results demonstrate that

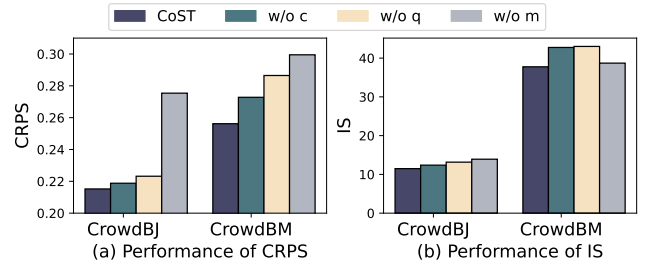


**Figure 3: Ablation study on the CrowdBJ and CrowdBM comparing variants in terms of (a) CRPS and (b) IS.**

**Table 5: Comparison of training time and sampling time on CellularSH dataset.**

Model	train time all	Inference time
D3VAE	3min 27s	2min 15s
DiffSTG	24min 16s	18min 38s
TimeGrad	5min	2min
CSDI	48min 40s	38min 49s
DyDiffusion	33h	3h
CoST	2min	50s

incorporating the conditional mean prediction module significantly enhances model performance, indicating that it effectively captures the primary spatiotemporal pattern and alleviates the burden on the diffusion model to capture the full data distribution. Furthermore, incorporating the customized fluctuation Scale as a prior condition further improves prediction performance, suggesting that it provides valuable fluctuation information across different regions. Finally, the scale-aware diffusion process enables the model to better utilize this condition.

### 5.5 Model Efficiency

We evaluated the training time of our model and all baseline models on the CellularSH dataset, as well as the time required to perform 50 sampling iterations on the test set. Notably, the pretraining time of the mean prediction module in our model is also included in the evaluation. The experimental results are summarized in Table 5. As shown in Table 5, our model demonstrates a significant advantage over existing probabilistic models in terms of training and inference efficiency. This efficiency is particularly valuable for real-world deployment scenarios. It is worth noting that while the CSDI model benefits from the Transformer architecture’s capability to capture spatiotemporal dependencies, its training and sampling time is considerably higher than that of other models, posing challenges for time-sensitive tasks.

### 5.6 Analysis of Distribution Alignment

For regions with complex distributions in the CellularSH dataset, we validate the model’s ability to capture multi-modal characteristics by comparing the predicted and true distributions using Kernel Density Estimation (KDE). As shown in Figure 4, the real distribution exhibits significant spatiotemporal multi-modality: Figure 4(a) shows three peaks, which likely represent values at different time points and values under different states at the same time points.

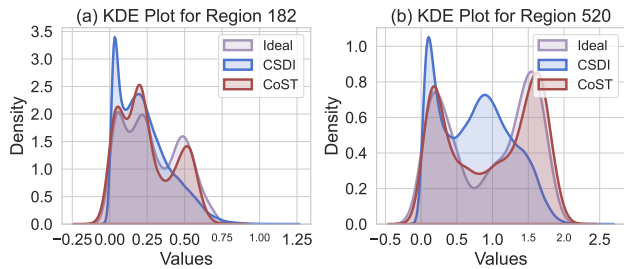


Figure 4: KDE plots of CellularSH dataset for different regions: (a) Location 182, (b) Location 520.

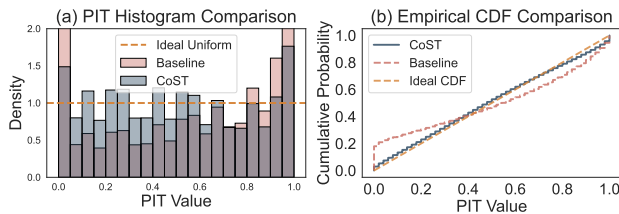


Figure 5: PIT analysis on the CellularSH dataset: (a) PIT histogram and (b) PIT empirical CDF.

CoST successfully captures the three peaks, while CSDI only fits two, demonstrating superior capability in modeling multimodal distributions. In Figure 4(b), the difference between the two peaks reflects strong temporal dynamics in this region. Although both models predict two peaks, the peak spacing of CoST is more consistent with the true distribution. These advantages stem from the model’s design: the diffusion model focuses on residuals, effectively capturing multimodal distribution features, while the deterministic model captures long-term trends and enhances the model’s capacity to model primary dynamic patterns.

Additionally, we present the PIT (Probability Integral Transform) histogram in Figure 5 (a) and the PIT empirical cumulative distribution function (CDF) in Figure 5 (b) to visually reflect the alignment of the full distribution. Ideally, the true values’ quantiles in the predictive distribution should follow a uniform distribution, corresponding to the dashed line in Figure 5 (a). In the case of perfect calibration, the PIT CDF should closely resemble the yellow diagonal line. Clearly, our model outperforms CSDI.

### 5.7 Analysis of Prediction Quality

To intuitively demonstrate the effectiveness of our predictions, we visualize the prediction results on the CrowdBJ dataset, as shown in Figure 6. Here, we compare our model with the best baseline model, CSDI. On one hand, thanks to the deterministic model, our model is able to more accurately capture regular spatiotemporal patterns, as demonstrated in Figures 6 (a, c, and f). On the other hand, the diffusion model, by focusing on modeling the residual distribution, better reflects the uncertainty in predictions across different samples, as illustrated in Figures 6 (b, d, g, and h).

In addition to sample-specific analysis, we also perform a comparative analysis of the prediction intervals against the best baseline model, CSDI. We visualize the dynamic quantile errors of the CrowdBM and CellularSH prediction results in Figure 7. For each

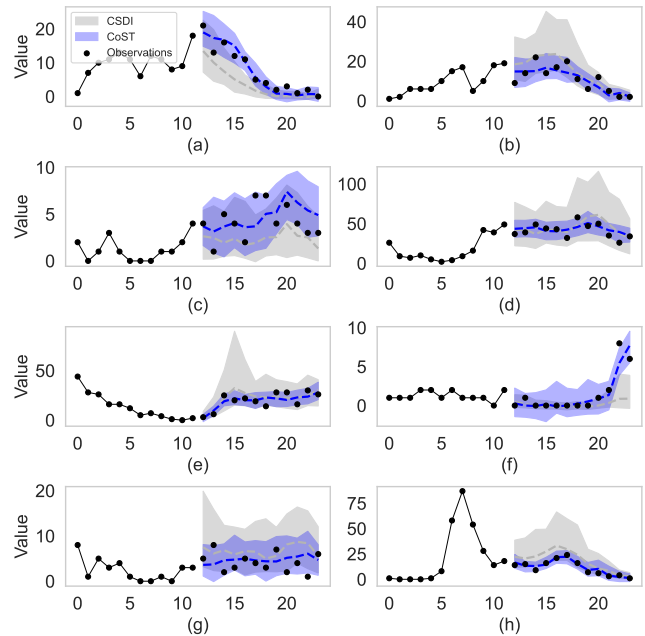


Figure 6: Visualizations of predictive uncertainty for both CSDI and our model on the CrowdBJ dataset. The shaded regions represent the 90% confidence interval, derived from 50 independent sampling runs. The dashed lines denote the median of the predicted values for each model.

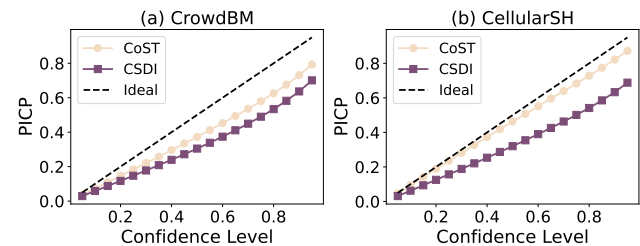


Figure 7: PICP comparison between our model and CSDI on CrowdBM and CellularSH.

confidence level  $\alpha$ , we compute the corresponding quantile intervals (e.g.,  $\frac{\alpha}{2}$  and  $1 - \frac{\alpha}{2}$ ) and calculate the proportion of real values falling within this interval, known as the Prediction Interval Coverage Probability (PICP). The closer the curve is to the diagonal (black dashed line), the better the calibration of the prediction intervals. The results show that our model achieves superior prediction interval calibration.

## 6 CONCLUSION

In this work, we propose to collaborate deterministic models and probabilistic models for effective probabilistic urban spatiotemporal predictions. By decomposing spatiotemporal data into conditional mean predicted by deterministic models and residual learned by diffusion models, bridging the gap between deterministic and probabilistic predictions, our CoST achieves dual advantages: precise



capture of primary patterns and non-linear variations. Experiments across seven real-world datasets demonstrate 20% performance gains over state-of-the-art baselines. This study provides an efficient solution for urban spatiotemporal prediction that balances pattern learning and uncertainty modeling, holding significant theoretical and practical value for smart city decision support.

## REFERENCES

- [1] Lei Bai, Lina Yao, Salil Kanhere, Xianzhi Wang, Quan Sheng, et al. 2019. Stg2seq: Spatial-temporal graph to sequence model for multi-step passenger demand forecasting. *arXiv preprint arXiv:1905.10069* (2019).
- [2] Lei Bai, Lina Yao, Salil S Kanhere, Zheng Yang, Jing Chu, and Xianzhi Wang. 2019. Passenger demand forecasting with multi-task convolutional recurrent neural networks. In *Advances in Knowledge Discovery and Data Mining: 23rd Pacific-Asia Conference, PAKDD 2019, Macau, China, April 14-17, 2019, Proceedings, Part II 23*. Springer, 29–42.
- [3] Lei Bai, Lina Yao, Can Li, Xianzhi Wang, and Can Wang. 2020. Adaptive graph convolutional recurrent network for traffic forecasting. *Advances in neural information processing systems* 33 (2020), 17804–17815.
- [4] Martin Behnisch and Alfred Ultsch. 2009. Urban data-mining: spatiotemporal exploration of multidimensional data. *Building Research & Information* 37, 5-6 (2009), 520–532.
- [5] Imad-Eddine Bouznad, Enrico Guastaldi, Andrea Zirulia, Mariantonietta Brancale, Alessio Barbagli, and Djamel Bengusmia. 2020. Trend analysis and spatiotemporal prediction of precipitation, temperature, and evapotranspiration values using the ARIMA models: case of the Algerian Highlands. *Arabian Journal of Geosciences* 13, 24 (2020), 1281.
- [6] Eoin Brophy, Zhengwei Wang, Qi She, and Tomas Ward. 2021. Generative adversarial networks in time series: A survey and taxonomy. *arXiv preprint arXiv:2107.11098* (2021).
- [7] Haoye Chai, Tao Jiang, and Li Yu. 2024. Diffusion Model-based Mobile Traffic Generation with Open Data for Network Planning and Optimization. In *Proceedings of the 30th ACM SIGKDD Conference on Knowledge Discovery and Data Mining*. 4828–4838.
- [8] Changlu Chen, Yanbin Liu, Ling Chen, and Chengqi Zhang. 2022. Bidirectional spatial-temporal adaptive transformer for urban traffic flow forecasting. *IEEE Transactions on Neural Networks and Learning Systems* 34, 10 (2022), 6913–6925.
- [9] Jiayuan Chen, Shuo Zhang, Xiaofei Chen, Qiao Jiang, Hejiao Huang, and Chonglin Gu. 2021. Learning traffic as videos: a spatio-temporal VAE approach for traffic data imputation. In *International Conference on Artificial Neural Networks*. Springer, 615–627.
- [10] Weihuang Chen, Fangfang Wang, and Hongbin Sun. 2021. S2tnet: Spatio-temporal transformer networks for trajectory prediction in autonomous driving. In *Asian conference on machine learning*. PMLR, 454–469.
- [11] Fernando Chirigati, Harish Doraiswamy, Theodoros Damoulas, and Juliana Freire. 2016. Data polygamy: The many-many relationships among urban spatiotemporal data sets. In *Proceedings of the 2016 International Conference on Management of Data*. 1011–1025.
- [12] Miguel Ángel De Miguel, José María Armingol, and Fernando Garcia. 2022. Vehicles trajectory prediction using recurrent VAE network. *IEEE Access* 10 (2022), 32742–32749.
- [13] Nan Gao, Hao Xue, Wei Shao, Sichen Zhao, Kyle Kai Qin, Arian Prabowo, Mohammad Saiedur Rahaman, and Flora D Salim. 2022. Generative adversarial networks for spatio-temporal data: A survey. *ACM Transactions on Intelligent Systems and Technology (TIST)* 13, 2 (2022), 1–25.
- [14] Qiang Gao, Xiaolong Song, Li Huang, Goce Trajcevski, Fan Zhou, and Xueqin Chen. 2024. Enhancing fine-grained urban flow inference via incremental neural operator. (2024).
- [15] Xu Geng, Yaguang Li, Leye Wang, Lingyu Zhang, Qiang Yang, Jieping Ye, and Yan Liu. 2019. Spatiotemporal multi-graph convolution network for ride-hailing demand forecasting. In *Proceedings of the AAAI conference on artificial intelligence*, Vol. 33. 3656–3663.
- [16] Tilmann Gneiting and Adrian E Raftery. 2007. Strictly proper scoring rules, prediction, and estimation. *Journal of the American statistical Association* 102, 477 (2007), 359–378.
- [17] Ian Goodfellow, Jean Pouget-Abadie, Mehdi Mirza, Bing Xu, David Warde-Farley, Sherjil Ozair, Aaron Courville, and Yoshua Bengio. 2020. Generative adversarial networks. *Commun. ACM* 63, 11 (2020), 139–144.
- [18] Kizewen Han, Huangjie Zheng, and Mingyuan Zhou. 2022. Card: Classification and regression diffusion models. *Advances in Neural Information Processing Systems* 35 (2022), 18100–18115.
- [19] Tomislav Hengl, Madlene Nussbaum, Marvin N Wright, Gerard BM Heuvelink, and Benedikt Gräler. 2018. Random forest as a generic framework for predictive modeling of spatial and spatio-temporal variables. *PeerJ* 6 (2018), e5518.
- [20] Jonathan Ho, Ajay Jain, and Pieter Abbeel. 2020. Denoising diffusion probabilistic models. *Advances in neural information processing systems* 33 (2020), 6840–6851.
- [21] Jiawei Jiang, Chengkai Han, Wayne Xin Zhao, and Jingyuan Wang. 2023. Pdfformer: Propagation delay-aware dynamic long-range transformer for traffic flow prediction. In *Proceedings of the AAAI conference on artificial intelligence*, Vol. 37. 4365–4373.
- [22] Guangyin Jin, Yuxuan Liang, Yuchen Fang, Zezhi Shao, Jincui Huang, Junbo Zhang, and Yu Zheng. 2023. Spatio-temporal graph neural networks for predictive learning in urban computing: A survey. *IEEE Transactions on Knowledge and Data Engineering* (2023).
- [23] Junchen Jin, Dingding Rong, Tong Zhang, Qingyuan Ji, Haifeng Guo, Yisheng Lv, Xiaoliang Ma, and Fei-Yue Wang. 2022. A GAN-based short-term link traffic prediction approach for urban road networks under a parallel learning framework. *IEEE Transactions on Intelligent Transportation Systems* 23, 9 (2022), 16185–16196.
- [24] Ming Jin, Shiyu Wang, Lintao Ma, Zhixuan Chu, James Y Zhang, Xiaoming Shi, Pin-Yu Chen, Yuxuan Liang, Yuan-Fang Li, Shirui Pan, et al. 2023. Time-llm: Time series forecasting by reprogramming large language models. *arXiv preprint arXiv:2310.01728* (2023).
- [25] Diederik P Kingma. 2013. Auto-encoding variational bayes. *arXiv preprint arXiv:1312.6114* (2013).
- [26] Ruiyuan Li, Huajun He, Rubin Wang, Yuchuan Huang, Junwen Liu, Sijie Ruan, Tianfu He, Jie Bao, and Yu Zheng. 2020. Just: Jd urban spatio-temporal data engine. In *2020 IEEE 36th International Conference on Data Engineering (ICDE)*. IEEE, 1558–1569.
- [27] Yan Li, Xinjiang Lu, Yaqing Wang, and Dejing Dou. 2022. Generative time series forecasting with diffusion, denoise, and disentanglement. *Advances in Neural Information Processing Systems* 35 (2022), 23009–23022.
- [28] Yaguang Li, Rose Yu, Cyrus Shahabi, and Yan Liu. 2017. Diffusion convolutional recurrent neural network: Data-driven traffic forecasting. *arXiv preprint arXiv:1707.01926* (2017).
- [29] Lequan Lin, Zhengkun Li, Ruikun Li, Xuliang Li, and Junbin Gao. 2024. Diffusion models for time-series applications: a survey. *Frontiers of Information Technology & Electronic Engineering* 25, 1 (2024), 19–41.
- [30] Zhihui Lin, Maomao Li, Zhuobin Zheng, Yangyang Cheng, and Chun Yuan. 2020. Self-attention convlstm for spatiotemporal prediction. In *Proceedings of the AAAI conference on artificial intelligence*, Vol. 34. 11531–11538.
- [31] Lingbo Liu, Ruimao Zhang, Jiefeng Peng, Guanbin Li, Bowen Du, and Liang Lin. 2018. Attentive crowd flow machines. In *Proceedings of the 26th ACM international conference on Multimedia*. 1553–1561.
- [32] Morteza Mardani, Noah Brenowitz, Yair Cohen, Jaideep Pathak, Chieh-Yu Chen, Cheng-Chin Liu, Arash Vahdat, Mohammad Amin Nabian, Tao Ge, Akshay Subramaniam, et al. 2023. Residual corrective diffusion modeling for km-scale atmospheric downscaling, 2024. URL <https://arxiv.org/abs/2309.15214> (2023).
- [33] Yuqi Nie, Nam H Nguyen, Phanwadee Sinthong, and Jayant Kalagnanam. 2022. A time series is worth 64 words: Long-term forecasting with transformers. *arXiv preprint arXiv:2211.14730* (2022).
- [34] Orlando Ohashi and Luis Torgo. 2012. Wind speed forecasting using spatio-temporal indicators. In *ECAI 2012*. IOS Press, 975–980.
- [35] Stephen B Pope. 2001. Turbulent flows. *Measurement Science and Technology* 12, 11 (2001), 2020–2021.
- [36] Yanjun Qin, Haiyong Luo, Fang Zhao, Yuchen Fang, Xiaoming Tao, and Chenxing Wang. 2023. Spatio-temporal hierarchical MLP network for traffic forecasting. *Information Sciences* 632 (2023), 543–554.
- [37] Kashif Rasul, Calvin Seward, Ingmar Schuster, and Roland Vollgraf. 2021. Autoregressive denoising diffusion models for multivariate probabilistic time series forecasting. In *International Conference on Machine Learning*. PMLR, 8857–8868.
- [38] Salva Rühling Cachay, Bo Zhao, Hailey Joren, and Rose Yu. 2023. Dyffusion: A dynamics-informed diffusion model for spatiotemporal forecasting. *Advances in neural information processing systems* 36 (2023), 45259–45287.
- [39] Divya Saxena and Jiannong Cao. 2019. D-GAN: Deep generative adversarial nets for spatio-temporal prediction. *arXiv preprint arXiv:1907.08556* (2019).
- [40] Ransalu Senanayake, Simon O’Callaghan, and Fabio Ramos. 2016. Predicting spatio-temporal propagation of seasonal influenza using variational Gaussian process regression. In *Proceedings of the AAAI conference on artificial intelligence*, Vol. 30.
- [41] Zezhi Shao, Zhao Zhang, Fei Wang, Wei Wei, and Yongjun Xu. 2022. Spatial-temporal identity: A simple yet effective baseline for multivariate time series forecasting. In *Proceedings of the 31st ACM International Conference on Information & Knowledge Management*. 4454–4458.
- [42] Zhi Sheng, Yuan Yuan, Jingtao Ding, and Yong Li. 2025. Unveiling the Power of Noise Priors: Enhancing Diffusion Models for Mobile Traffic Prediction. *arXiv preprint arXiv:2501.13794* (2025).
- [43] Yusuke Tashiro, Jiaming Song, Yang Song, and Stefano Ermon. 2021. Csd: Conditional score-based diffusion models for probabilistic time series imputation. *Advances in Neural Information Processing Systems* 34 (2021), 24804–24816.
- [44] Yunbo Wang, Zhifeng Gao, Mingsheng Long, Jianmin Wang, and S Yu Philip. 2018. Predrnn++: Towards a resolution of the deep-in-time dilemma in spatiotemporal

- predictive learning. In *International conference on machine learning*. PMLR, 5123–5132.
- [45] Yunbo Wang, Mingsheng Long, Jianmin Wang, Zhifeng Gao, and Philip S Yu. 2017. Predrnn: Recurrent neural networks for predictive learning using spatiotemporal lstms. *Advances in neural information processing systems* 30 (2017).
- [46] Haomin Wen, Youfang Lin, Yutong Xia, Huaiyu Wan, Qingsong Wen, Roger Zimmermann, and Yuxuan Liang. 2023. Diffstg: Probabilistic spatio-temporal graph forecasting with denoising diffusion models. In *Proceedings of the 31st ACM International Conference on Advances in Geographic Information Systems*. 1–12.
- [47] Peng Xie, Tianrui Li, Jia Liu, Shengdong Du, Xin Yang, and Junbo Zhang. 2020. Urban flow prediction from spatiotemporal data using machine learning: A survey. *Information Fusion* 59 (2020), 1–12.
- [48] Sijie Yan, Yuanjun Xiong, and Dahua Lin. 2018. Spatial temporal graph convolutional networks for skeleton-based action recognition. In *Proceedings of the AAAI conference on artificial intelligence*, Vol. 32.
- [49] Yiyuan Yang, Ming Jin, Haomin Wen, Chaoli Zhang, Yuxuan Liang, Lintao Ma, Yi Wang, Chenghao Liu, Bin Yang, Zenglin Xu, et al. 2024. A survey on diffusion models for time series and spatio-temporal data. *arXiv preprint arXiv:2404.18886* (2024).
- [50] Bing Yu, Haoteng Yin, and Zhanxing Zhu. 2017. Spatio-temporal graph convolutional networks: A deep learning framework for traffic forecasting. *arXiv preprint arXiv:1709.04875* (2017).
- [51] Cunjun Yu, Xiao Ma, Jiawei Ren, Haiyu Zhao, and Shuai Yi. 2020. Spatio-temporal graph transformer networks for pedestrian trajectory prediction. In *Computer Vision—ECCV 2020: 16th European Conference, Glasgow, UK, August 23–28, 2020, Proceedings, Part XII* 16. Springer, 507–523.
- [52] Yuan Yuan, Jingtao Ding, Jie Feng, Depeng Jin, and Yong Li. 2024. Unist: A prompt-empowered universal model for urban spatio-temporal prediction. In *Proceedings of the 30th ACM SIGKDD Conference on Knowledge Discovery and Data Mining*. 4095–4106.
- [53] Yuan Yuan, Jingtao Ding, Chonghua Han, Depeng Jin, and Yong Li. 2024. A Foundation Model for Unified Urban Spatio-Temporal Flow Prediction. *arXiv preprint arXiv:2411.12972* (2024).
- [54] Yuan Yuan, Jingtao Ding, Chenyang Shao, Depeng Jin, and Yong Li. 2023. Spatio-temporal diffusion point processes. In *Proceedings of the 29th ACM SIGKDD Conference on Knowledge Discovery and Data Mining*. 3173–3184.
- [55] Junbo Zhang, Yu Zheng, and Dekang Qi. 2017. Deep spatio-temporal residual networks for citywide crowd flows prediction. In *Proceedings of the AAAI conference on artificial intelligence*, Vol. 31.
- [56] Liang Zhang, Jianqing Wu, Jun Shen, Ming Chen, Rui Wang, Xinliang Zhou, Cankun Xu, Quankai Yao, and Qiang Wu. 2021. SATP-GAN: Self-attention based generative adversarial network for traffic flow prediction. *Transportmetrica B: Transport Dynamics* 9, 1 (2021), 552–568.
- [57] Zijian Zhang, Ze Huang, Zhiwei Hu, Xiangyu Zhao, Wanyu Wang, Zitao Liu, Junbo Zhang, S Joe Qin, and Hongwei Zhao. 2023. MLPST: MLP is All You Need for Spatio-Temporal Prediction. In *Proceedings of the 32nd ACM International Conference on Information and Knowledge Management*. 3381–3390.
- [58] Fan Zhou, Qing Yang, Ting Zhong, Dajiang Chen, and Ning Zhang. 2020. Variational graph neural networks for road traffic prediction in intelligent transportation systems. *IEEE Transactions on Industrial Informatics* 17, 4 (2020), 2802–2812.

## APPENDIX

**Table 6: The basic information of grid-based spatio-temporal data.**

Dataset	City	Type	Temporal Period	Spatial partition	Interval	Mean	Std
TaxiBJ	Beijing	Taxi flow	2014/03/01 - 2014/06/30	32 × 32	Half an hour	111.5	139.3
BikeDC	Washington, D.C.	Bike flow	2010/09/20 - 2010/10/20	20 × 20	Half an hour	0.924	4.88
CellularSH	Shanghai	Cellular traffic	2014/08/01 - 2014/08/21	32 × 28	One hour	0.175	0.212
CellularNJ	Nanjing	Cellular traffic	2021/02/02 - 2021/02/22	20 × 28	One hour	0.842	1.30
CrowdBJ	Beijing	Crowd flow	2018/01/01 - 2018/01/31	1010	One hour	7.07	11.1
CrowdBM	Baltimore	Crowd flow	2019/01/01 - 2019/05/31	403	One hour	14.4	29.3
Los-Speed	Los Angeles	Traffic speed	2012/03/01 - 2012/03/07	207	Five minutes	59.0	12.5

**Table 7: Short-term prediction results on two additional datasets in terms of both deterministic and probabilistic metrics. Bold indicates the best performance, while underlining denotes the second-best.**

Model	CellularNJ					CrowdBM				
	MAE	RMSE	CRPS	QICE	IS	MAE	RMSE	CRPS	QICE	IS
D3VAE	0.580	1.135	0.565	0.096	6.03	11.0	24.7	0.593	0.110	136.4
DiffSTG	0.317	0.649	0.291	0.071	3.11	8.88	21.3	0.453	0.047	68.5
TimeGrad	0.340	0.357	0.432	0.162	5.87	10.1	<u>12.4</u>	<b>0.240</b>	<u>0.085</u>	<u>46.9</u>
CSDI	0.129	0.237	<u>0.111</u>	<u>0.039</u>	<u>0.80</u>	7.31	19.3	0.390	0.054	61.1
NPDiff	<u>0.123</u>	<u>0.175</u>	0.128	0.133	2.22	<u>5.42</u>	13.7	0.331	0.119	91.2
DyDiffusion	0.222	0.357	0.196	0.080	1.80	-	-	-	-	-
<b>CoST</b>	<b>0.102</b>	<b>0.172</b>	<b>0.090</b>	<b>0.037</b>	<b>0.682</b>	<b>5.04</b>	<b>12.1</b>	<u>0.256</u>	<b>0.027</b>	<b>37.8</b>